

p63 is a cereblon substrate involved in thalidomide teratogenicity

Tomoko Asatsuma-Okumura^{1,5}, Hideki Ando^{1,5}, Marco De Simone², Junichi Yamamoto¹, Tomomi Sato¹, Nobuyuki Shimizu¹, Kazuhide Asakawa¹, Yuki Yamaguchi³, Takumi Ito^{1,4}, Luisa Guerrini^{2*} and Hiroshi Handa^{1*}

Cereblon (CRBN) is a primary target of thalidomide and mediates its multiple pharmacological activities, including teratogenic and antimyeloma activities. CRBN functions as a substrate receptor of the E3 ubiquitin ligase CRL4, whose substrate specificity is modulated by thalidomide and its analogs. Although a number of CRL4^{CRBN} substrates have recently been identified, the substrate involved in thalidomide teratogenicity is unclear. Here we show that p63 isoforms are thalidomide-dependent CRL4^{CRBN} neosubstrates that are responsible, at least in part, for its teratogenic effects. The p53 family member p63 is associated with multiple developmental processes. Δ Np63 α is essential for limb development, while TAp63 α is important for cochlea development and hearing. Using a zebrafish model, we demonstrate that thalidomide exerts its teratogenic effects on pectoral fins and otic vesicles by inducing the degradation of Δ Np63 α and TAp63 α , respectively. These results may contribute to the invention of new thalidomide analogs lacking teratogenic activity.

Thalidomide was originally used to relieve morning sickness and caused serious congenital birth defects in the early 1960s^{1,2}. Thalidomide-induced birth defects are characterized by a distinctive pattern of abnormalities affecting various organs, including limb deformities such as phocomelia and amelia, ear malformations, bowel atresia, cranial nerve dysfunction and malformations of the heart, kidneys, genital tracts and intestine¹. After being withdrawn from the market, further studies revealed new potentially therapeutic activities of thalidomide and its derivatives. This led to the approval of thalidomide for the treatment of leprosy and multiple myeloma in 1998 and 1999, respectively³. These findings also led to the development of thalidomide derivatives that are collectively called immunomodulatory drugs.

For decades, little was known about the molecular mechanisms of action of thalidomide and its derivatives until we identified CRBN as a primary target of thalidomide⁴. CRBN, together with DDB1 and Cul4, forms an E3 ubiquitin ligase complex called cullin-4 ubiquitin ligase 4 (CRL4^{CRBN})⁵. In the previous study, we have demonstrated using zebrafish and chicken embryos that CRBN mediates thalidomide-induced limb and ear defects. Fgf8, a key regulator for limb development, is expressed in the apical ectodermal ridge (AER) of developing limb buds and is necessary for proximodistal outgrowth of developing limb buds^{6,7}. Thalidomide treatment abolishes Fgf8 expression in a CRBN-dependent manner in zebrafish pectoral fins and chicken forelimbs⁴. Nevertheless, the mechanism linking the thalidomide–CRL4^{CRBN} pathway to Fgf8 downregulation in the AER and to other teratogenic phenotypes remains unclear.

Recent biochemical and pharmacological studies of the anticancer activity of thalidomide and its derivatives have led to the identification of numerous drug-dependent neosubstrates of CRL4^{CRBN}, such as Ikaros, Aiolos, CK1 α , GSPT1, GFP91 and SALL4. These factors bind to CRBN and are targeted for ubiquitination and degradation only in the presence of immunomodulatory drugs, which

serve as molecular glues between the enzyme and the substrates^{8–14}. However, little is known about the mechanism of the teratogenic side-effects of thalidomide. Phenotypic similarities between thalidomide-exposed newborns and patients carrying mutations in the p63 gene (*TP63*)¹⁵ prompted us to investigate whether p63 is involved in the thalidomide–CRL4^{CRBN} pathway. In the AER, Fgf8 is part of a complex pathway involving p63, a member of the p53 transcription factor family^{16,17}. In humans, *TP63* mutations result in several disorders that are characterized by congenital limb malformations, ectodermal dysplasias and facial clefts. *TP63*-null mouse embryos display malformations of epithelial derivatives including limbs, tail, urogenital structures, brain, face and teeth^{18,19}. Alternative promoter usage and alternative splicing of *TP63* result in the production of more than ten isoforms with different N and C termini, TAp63 α and Δ Np63 α are main isoforms with differential expression patterns and developmental functions. TAp63 α is essential for heart and ear development and oocyte maintenance^{18–20}, whereas Δ Np63 α is essential for AER maintenance and limb outgrowth^{16,17}.

In this study, we show that p63 isoforms Δ Np63 α and TAp63 α are neosubstrates of CRL4^{CRBN} and are targeted for degradation in the presence of thalidomide. Using zebrafish, we show that characteristic features of thalidomide embryopathy, such as limb or ear malformations, are caused by thalidomide-dependent degradation of Δ Np63 and TAp63, respectively.

Results

Δ Np63 α and TAp63 α are CRL4^{CRBN} neosubstrates. Given the phenotypic similarity between *TP63*-related disorders and thalidomide embryopathy, we examined whether p63 serves as a thalidomide-dependent neosubstrate of CRL4^{CRBN}. Here keratinocyte-derived HaCat cells were used because RNA sequencing data in the past suggested that *TP63* is expressed at a high level in this cell line. Thalidomide treatment of human HaCat cells resulted in a

¹Department of Nanoparticle Translational Research, Tokyo Medical University, Shinjuku-ku, Tokyo, Japan. ²Department of Biosciences, Università degli Studi di Milano, Milan, Italy. ³School of Life Science and Technology, Tokyo Institute of Technology, Yokohama, Japan. ⁴PRESTO, JST, 4-1-8 Honcho, Kawaguchi, Japan. ⁵These authors contributed equally: Tomoko Asatsuma-Okumura, Hideki Ando. *e-mail: luisa.guerrini@unimi.it; handa@tokyo-med.ac.jp

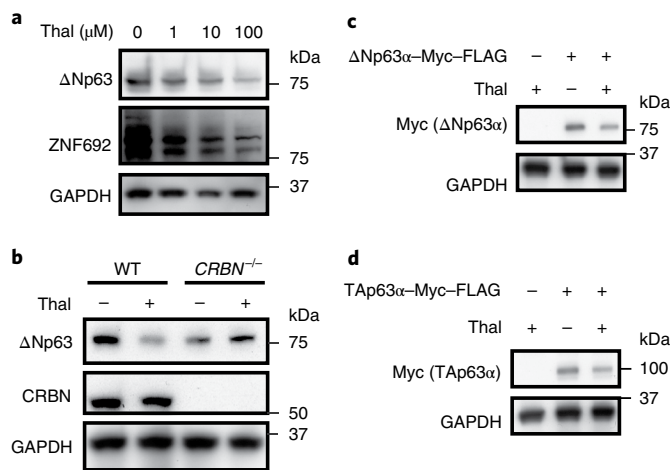


Fig. 1 | Δ Np63 α and TAp63 α are downstream factors of the thalidomide-CRL4^{CRBN} pathway. **a**, Immunoblot analysis of whole cell extracts of HaCat cells incubated with DMSO or indicated concentration of thalidomide for 24 h ($n=9$, biological replicates). Thal, thalidomide. **b**, The effect of thalidomide on p63 protein levels in wild-type (WT) and CRBN^{-/-} HaCat cells ($n=9$, biological replicates). **c,d**, The effect of thalidomide on Δ Np63 α or TAp63 α overexpressed in HEK293T cells expressing FLAG-hemagglutinin (HA)-CRBN ($n=5$, biological replicates). Full images of all blots in this figure are shown in Supplementary Fig. 8.

concentration- and time-dependent decrease of Δ Np63 α proteins, while it had little effect on levels of mRNA encoding p63 (Fig. 1a and Supplementary Fig. 1a–c). The decrease of Δ Np63 α by thalidomide was detectable at concentrations as low as 1 μ M. In CRBN-depleted HaCat cells, however, the Δ Np63 α protein level was not downregulated appreciably by thalidomide (Fig. 1b). While expression of the TAp63 α isoform was hardly detectable in undifferentiated HaCat cells, its expression was elevated upon the induction of differentiation, as reported previously^{21,22}, and was reduced by thalidomide treatment (Supplementary Fig. 1d). Moreover, TAp63 α expression was not affected by thalidomide treatment in CRBN-depleted HaCat cells (Supplementary Fig. 1d), suggesting that thalidomide-induced downregulation of Δ p63 α and TAp63 α is dependent on CRBN. To confirm this finding, Δ Np63 α and TAp63 α were ectopically expressed in HEK293T cells, in which the endogenous TP63 gene is not expressed (Supplementary Fig. 1e). As a result, production of both isoforms was downregulated by thalidomide treatment (Fig. 1c,d). These data indicate that both Δ Np63 α and TAp63 α are downstream factors of the thalidomide-CRL4^{CRBN} pathway.

We next investigated whether the decrease in p63 protein levels upon thalidomide treatment results from CRL4^{CRBN}-dependent ubiquitination and proteasomal degradation. Thalidomide-induced reduction of Δ Np63 α protein levels was prevented by simultaneous treatment with the proteasome inhibitor MG132 (Fig. 2a) or the neddylation inhibitor MLN4924 (Fig. 2b). Moreover, thalidomide shortened the half-life of the Δ Np63 α protein (Fig. 2c), suggesting that p63 proteins are thalidomide-dependent neosubstrates of CRL4^{CRBN}. To explore this idea further, we performed cell-based ubiquitination assays using Δ Np63 α or TAp63 α overexpressed in HEK293T cells. Six-hour treatment with thalidomide and MG132 induced accumulation of ubiquitinated p63 proteins in control HEK293T cells (Fig. 2d), but not in CRBN-depleted cells (Supplementary Fig. 1f). Moreover, co-immunoprecipitation studies using recombinant proteins suggested that both Δ Np63 α and TAp63 α weakly interact with CRBN in the absence of thalidomide and that their interactions are stabilized by thalidomide (Fig. 2e and

Supplementary Fig. 1g), leading us to conclude that these TP63 gene products are thalidomide-dependent neosubstrates of CRL4^{CRBN}.

To generalize the above findings, we examined whether similar results are obtained using various cell types. Expression of TP63 is tissue-specific and was undetectable in many cell lines including those previously used to identify neosubstrates such as HEK293T, HCT116 and MM.1S cells (Supplementary Fig. 1e,h–j). However, we detected p63 proteins in some cell lines and confirmed a thalidomide-dependent decrease in p63 protein levels in melanoma A375-C5 cells and human cardiac myocytes (Supplementary Fig. 1k). The restricted expression pattern of p63 may account, in part, for why p63 proteins were not identified as neosubstrates in previous studies. Recently, SALL4 was identified as a thalidomide-dependent neosubstrate that may be involved in thalidomide embryopathy^{13,14}. While SALL4 was not expressed in HaCat cells, thalidomide-induced degradation of SALL4 was confirmed in induced pluripotent stem cells (Supplementary Fig. 1l). Conversely, p63 was not expressed at a detectable level in induced pluripotent stem cells (Supplementary Fig. 1j,l), suggesting that thalidomide-induced degradation of p63 and SALL4 occurs independently.

Δ Np63 α mediates thalidomide-induced fin defects. We next investigated if p63 degradation is involved in thalidomide teratogenicity. To this end, we adopted zebrafish as an experimental animal, as it has several advantages for this study. First, rapid embryonic development and optical transparency of the embryos allow easy monitoring of developmental processes. Second, knockdown of genes of interest can be easily conducted using morpholino-antisense oligonucleotides²³. Third, zebrafish has a CRBN homolog, zCRBN, which is 70% homologous to human CRBN⁴, and several groups have independently shown that zebrafish are sensitive to thalidomide^{4,24,25}. To determine whether the thalidomide-dependent interaction between p63 and CRBN is evolutionarily conserved, we cloned zebrafish homologs of Δ Np63 α and TAp63 α (Supplementary Fig. 2) and transiently overexpressed them together with zCRBN in HEK293T CRBN^{-/-} cells for co-immunoprecipitation studies. Thalidomide increased the interaction of zCRBN with both Δ Np63 α and zTAp63 α (Supplementary Fig. 3a), indicating that the thalidomide-CRL4^{CRBN}-p63 pathway is conserved between humans and zebrafish. On the other hand, zCRBN did not interact with zSALL4 even in the presence of thalidomide (Supplementary Fig. 3b), as reported previously¹³, suggesting that SALL4 is not involved in thalidomide teratogenicity in zebrafish. Moreover, physical interactions between p63 and SALL4 were not observed (Supplementary Fig. 3c), suggesting that these factors function independently of each other. Δ Np63 α is known to be essential for fin development in zebrafish; its knockdown results in loss of pectoral fins, while its overexpression results in truncation of the anterior central nervous system with defects in forebrain and eyes²⁶. Concordantly, knockdown of Δ Np63 mediated by morpholino-antisense oligonucleotides induced serious defects of pectoral fin outgrowth (Fig. 3a and Supplementary Fig. 4a). By contrast, overexpression or knockdown of zTAp63 did not cause fin malformation (Fig. 3a). Given these findings, we investigated if overexpression of Δ Np63 α suppresses the teratogenic effects of thalidomide. Overexpression of Δ Np63 α reversed the thalidomide-induced defects in pectoral fins (Fig. 3b–e). Coincidentally, thalidomide-induced downregulation of zFgf8 expression was also reversed by Δ Np63 α overexpression, but not by zTAp63 α overexpression (Fig. 3f and Supplementary Fig. 4b).

As Δ Np63 α overexpression induces truncation of the anterior central nervous system as described above, there is a concern that head truncation might indirectly affect fin morphology. To eliminate unwanted effects of knockdown or thalidomide treatment, we directly injected thalidomide solution, vivo morpholino (VMO) or an mRNA-lipid complex into the left pectoral fin field of 24-hours-post-fertilization (hpf) embryos²⁷ (Supplementary Fig. 5a).

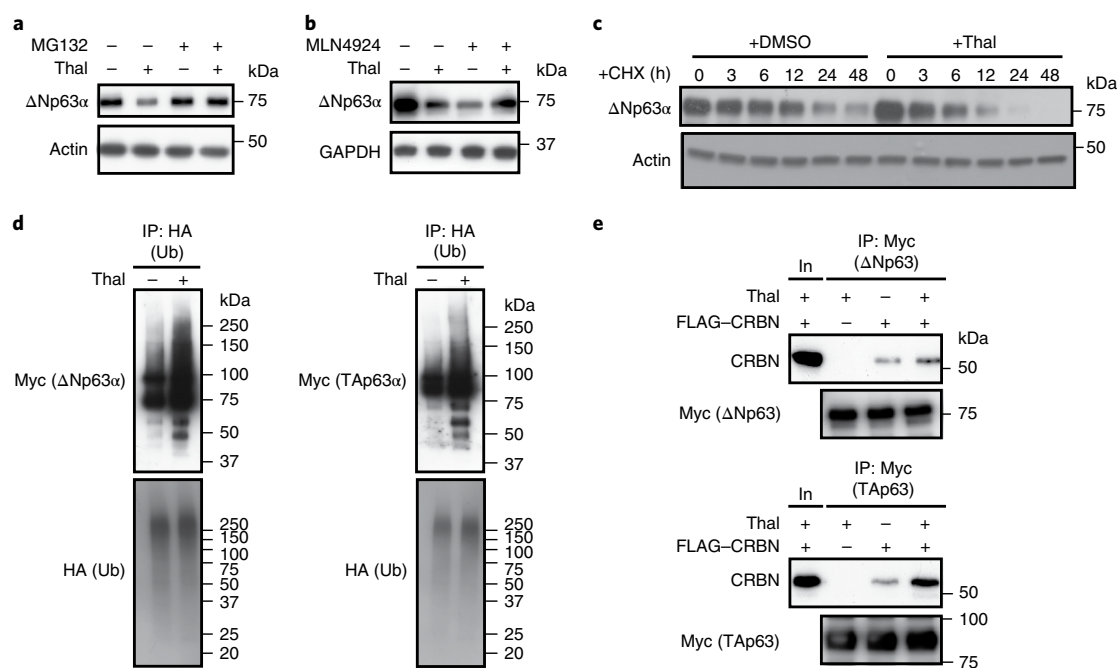


Fig. 2 | Δ Np63 α and TAp63 α are neosubstrates of CRL4^{CRBN}. **a, b**, HaCat cells were incubated with DMSO or thalidomide for 24 h and harvested for immunoblot analysis. Where indicated, 10 μ M MG132 (**a**) or 0.1 μ M MLN4924 (**b**) was added 6 h before cells were collected ($n=3$, biological replicates). **c**, Immunoblot analysis of HaCat cells treated with 50 μ g ml⁻¹ cycloheximide (CHX) and DMSO or thalidomide for the indicated periods ($n=3$, biological replicates). **d**, HEK293T cells overexpressing Myc-tagged Δ Np63 α (left) or TAp63 α (right) and HA-tagged ubiquitin (Ub) were treated with thalidomide and MG132 for 6 h and subjected to immunoprecipitation (IP) with anti-HA beads ($n=3$, biological replicates). **e**, Interactions of Myc-tagged Δ Np63 α and TAp63 α with FLAG-tagged CRBN in the absence or presence of thalidomide were analyzed by co-immunoprecipitation ($n=2$, biological replicates). Full images of all blots in this figure are shown in Supplementary Fig. 8.

Direct injection of thalidomide resulted in a significant malformation of the left, but not right, pectoral fin at 72 hpf (Fig. 4a). Severity of fin malformation was concentration dependent, and thalidomide caused fin defects at concentrations as low as 5 μ M. This observation is in contrast to the high concentrations required to induce similar defects by waterborne exposure⁴; this conflict may be due to a low penetration efficiency of the drug into the embryos. In any case, considering that thalidomide solution is diluted with body fluid after injection, its effective concentration must be lower than 5 μ M, which is below the maximum plasma concentration of orally administered thalidomide in humans (5.4 μ M at 1.95 to 3.85 mg kg⁻¹)²⁸. As expected, injection of z Δ Np63 VMO into the left pectoral fin field caused similar fin malformation (Supplementary Fig. 5b). Simultaneous injection of mRNA encoding z Δ Np63 α mRNA, but not of mRNA encoding zTAp63 α , reversed the effect of thalidomide on fin development without causing any adverse effect on head development (Fig. 4b), suggesting that z Δ Np63 α is a critical downstream target of thalidomide teratogenicity.

Zebrafish embryos that received thalidomide at 24 hpf showed a higher incidence of the severe phenotype than embryos that received thalidomide at 48 hpf (Supplementary Fig. 5c). To look more closely at thalidomide-induced phenotypes, we conducted Alcian blue staining to visualize chondrogenic differentiation. Approximately 40 embryos were examined per condition at 75 hpf, and approximately 70% of the embryos displayed the phenotypes shown in Supplementary Fig. 5d. As reported previously⁴, thalidomide severely impaired chondrogenesis of pectoral fins, and the effect was more profound when thalidomide was injected earlier. More specifically, thalidomide injection at 48 hpf resulted in a partial reduction in the size of endoskeletal disc with little or no reduction in the size of scapulocoracoid and cleithrum. Thalidomide injection at 24 hpf resulted in severe defects in chondrogenesis, with

the absence of cleithrum and endoskeletal disc. These results are consistent with the fact that mesenchymal proliferation, outgrowth of the fin bud and chondrogenesis actively take place in this period. The effect of thalidomide on chondrogenesis appeared to be more profound and more consistent than its effect on the length of pectoral fins, suggesting that defective chondrogenesis may be an underlying cause of thalidomide-induced fin malformations. Although it is difficult to associate endoskeletal elements of zebrafish pectoral fins with those of human forelimbs, the scapulocoracoid and the cleithrum correspond to the shoulder girdle in humans while the endoskeletal disc corresponds to the human arm such as stylopod, autopod and zeugopod. Thus, forelimb deformities found in thalidomide embryopathy may be paralleled with defective endoskeletal disc formation in pectoral fins.

Fgf8 is a critical regulator of limb development whose function is conserved from zebrafish to humans, and accumulating studies have shown that its downregulation leads to the induction of pro-apoptotic genes and causes cell death in limbs^{6,29}. As thalidomide treatment results in downregulation of zFgf8⁴ (Supplementary Fig. 4b), Fgf8 is a plausible downstream mediator of the thalidomide-CRL4^{CRBN}-p63 pathway. To fill the gaps of this scenario, we performed two sets of experiments. First, we showed that the knockdown of Δ Np63 also results in downregulation of zFgf8 (Supplementary Fig. 5e). Second, we showed that the knockdown of Δ Np63, as well as thalidomide treatment, causes apoptosis in a spatially restricted manner upon injection into the left pectoral fin field (Supplementary Fig. 5f,g). These results support the idea that thalidomide-induced degradation of z Δ Np63 triggers apoptosis through zFgf8 downregulation in the developing fin bud.

Next, we sought to employ nondegradable mutants of p63. Previous studies have shown that single point mutations in CRBN neosubstrates at a specific glycine residue confer resistance to

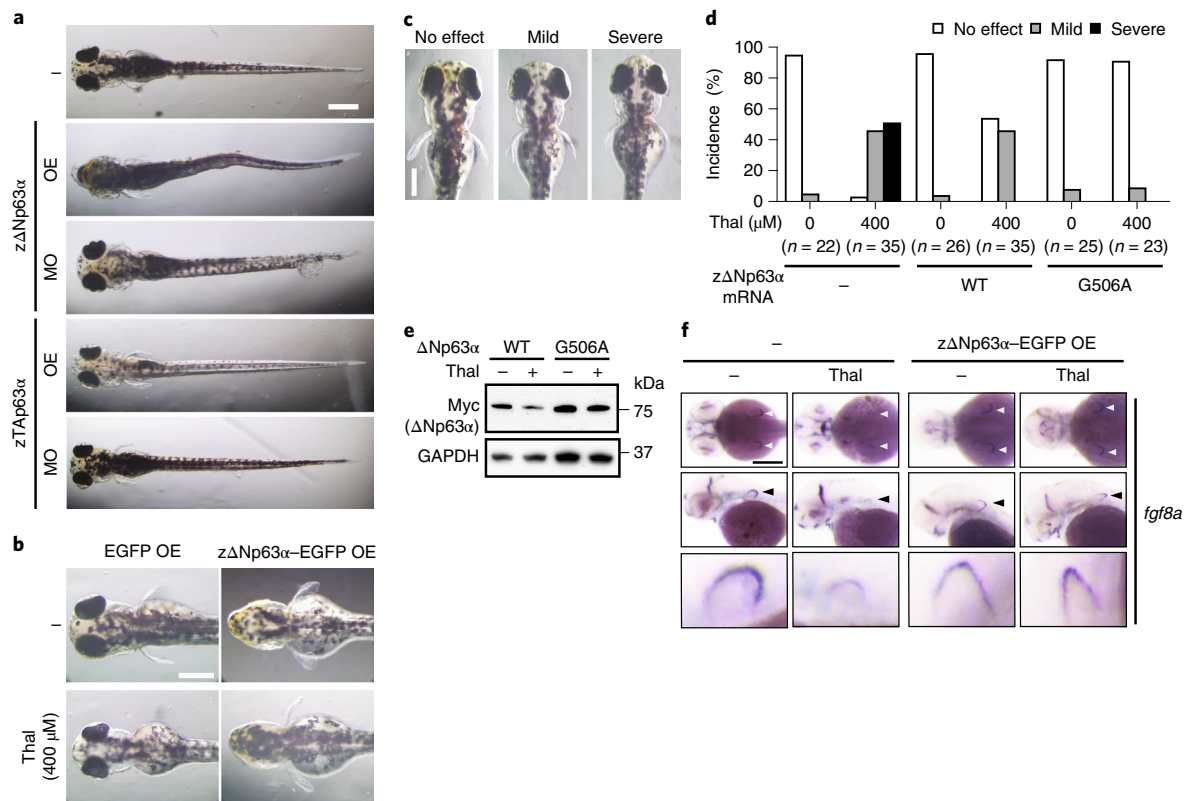


Fig. 3 | Overexpression of zΔNp63 reverses thalidomide-induced fin malformation in zebrafish. **a**, Dorsal views of larvae 5 d post fertilization that were uninjected or injected with mRNAs or morpholino oligonucleotides for zΔNp63 and zTAp63. OE, overexpression. Scale bar, 300 μm. $n = 26$ –37 zebrafish in each group. **b**, Dorsal views of 72-hours-post-fertilization (hpf) embryos. Embryos injected with EGFP or mRNA encoding zΔNp63-EGFP were allowed to develop in the presence or absence of thalidomide. Scale bar, 300 μm. $n = 22$ –35 zebrafish in each group. **c**, Phenotypes of pectoral fins were classified into three groups. Specifically, the length between the most proximal end of endoskeletal disks and the most distal end of actinotrichia was measured, and fins that were stretched out from the body wall and were more than 85% of control fins in length were defined as ‘no effect.’ Fins that were stretched out but were 60–85% of control fins were defined as ‘mild’, whereas fins that showed disk-like morphology and were less than 60% of control fins were defined as ‘severe’. Representative phenotypes are shown. Scale bar, 300 μm. **d**, Incidence of fin malformations in 72-hpf embryos uninjected (–) or injected with mRNA encoding wild-type zΔNp63 or a G506A variant. Each phenotype was classified on the basis of the criteria shown in **c**. **e**, HEK293T cells overexpressing wild-type human ΔNp63α or a G506A variant were treated with DMSO or thalidomide and collected for immunoblot analysis ($n = 3$, biological replicates). Full images of blots are shown in Supplementary Fig. 8. **f**, Whole-mount in situ hybridization for *fgf8a*. Shown are dorsal (top) and lateral (middle) views of 48-hpf embryos uninjected (–) or injected with mRNA encoding zΔNp63 and developed in the presence or absence of thalidomide. Pectoral fins are indicated with arrowheads. A higher magnification of the fin is shown at the bottom. Scale bar, 300 μm. $n = 35$ –41 zebrafish for each group.

drug-induced ubiquitination and degradation^{11,12,30}. Human ΔNp63γ, a splice variant lacking the C-terminal 231-amino-acid region of human ΔNp63α (amino acids 356–586), was not affected by thalidomide treatment (Supplementary Fig. 6a), while the deletion mutant α-γ spanning amino acids 330–586 of ΔNp63α was slightly decreased by thalidomide (Supplementary Fig. 6b). To identify a critical glycine residue(s), we substituted glycine residues within this region individually and found that ΔNp63α G506A is resistant to degradation by thalidomide (Fig. 3e and Supplementary Fig. 6b). G506 is a surface residue of the sterile α-motif (SAM) domain of ΔNp63α, which is thought to be involved in protein–protein interactions. To test whether the overall structure of the point mutant is intact, we conducted two sets of experiments. First, we studied the interaction between p63 and HDAC2, which is known to involve the C-terminal α-specific region of p63³¹, and found that this interaction was not affected by the G-to-A substitution appreciably (Supplementary Fig. 6c). Moreover, the nuclear localization of p63 was unaffected by the G-to-A mutation (Supplementary Fig. 6d). Note, however, that we cannot entirely exclude the possibility that the mutation disrupts the structure of the SAM domain, because HDAC2 binding and nuclear localization are not dependent on the SAM domain.

As this glycine residue is conserved among vertebrates, the corresponding mutant of zΔNp63α was used for overexpression experiments in zebrafish. When zebrafish eggs injected with the same amounts of mRNAs encoding wild-type or G506A zΔNp63α were allowed to develop in the presence or absence of thalidomide, embryos overexpressing the nondegradable mutant developed normal pectoral fins at a higher rate than embryos overexpressing wild-type zΔNp63α in the presence of thalidomide (Fig. 3d). These findings are consistent with the idea that thalidomide-induced degradation of ΔNp63α drives fin malformations.

zTAp63α mediates thalidomide-induced ear defects. We next investigated the potential role of p63 in thalidomide-induced defects of otic vesicles (ears). In mice, TAp63 is reportedly critical for ear development and is associated with sensorineural deafness¹⁹. First, we examined whether TAp63 is involved in otic development in zebrafish. Knockdown of zTAp63 using morpholino-antisense oligonucleotides resulted in a twofold reduction of otic vesicle size in diameter, and this reduction was reversed by the simultaneous injection of mRNA encoding zTAp63α (Supplementary Fig. 7a,b). We therefore investigated the effect of TAp63 knockdown on the

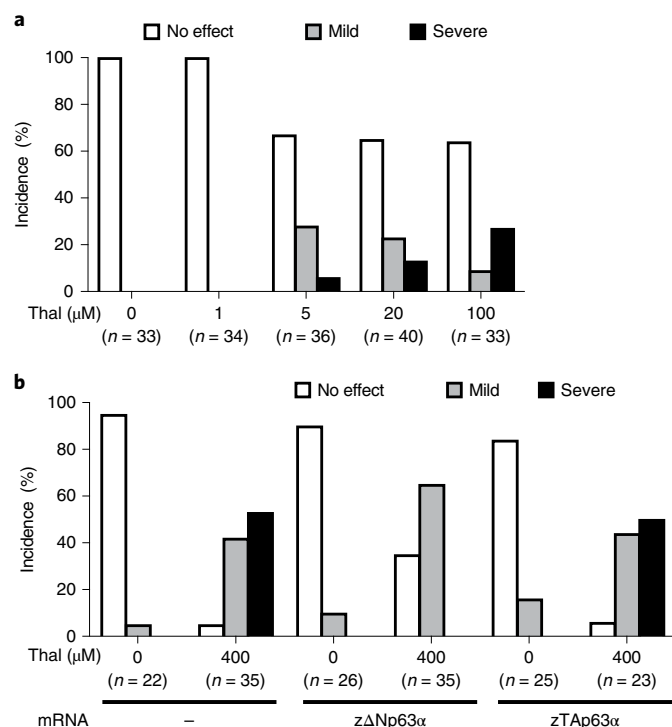


Fig. 4 | zΔNp63, but not zTAp63, suppresses fin malformations in zebrafish. a, Incidence of developmental defects in the left pectoral fin of 72-hpf embryos that received in vivo thalidomide treatment. A solution containing 5 μM thalidomide was injected into the left pectoral fin field at 24 hpf. **b**, Incidence of developmental defects in the left pectoral fin of 72-hpf embryos that received in vivo lipofection (IVL). Phenotypes were classified according to the criteria shown in Fig. 3c.

expression of *pax2a* and *atoh1a*. Pax2a is a transcription factor that functions in specification and patterning of otic vesicles³² while Atoh1 is a transcription factor that is essential for the development of sensory neurons and cochlea and is reported as one of the downstream targets of TAp63 in mice¹⁹. The mRNA levels of *pax2a* and *atoh1a* were both reduced by TAp63 knockdown and were restored by simultaneous injection of mRNA encoding zTAp63α (Supplementary Fig. 7c,d). These results suggest that TAp63 is critical for an early stage of otic development in zebrafish. Next, as we have shown that ΔNp63α and TAp63α are similarly degraded by CRL4^{CRBN} upon thalidomide treatment, we examined whether thalidomide-mediated inhibition of otic vesicle development is reversed by the overexpression of zΔNp63α or zTAp63α. Thalidomide reduced otic vesicle size by 50%, and this reduction was reversed by overexpression of wild-type zTAp63α or its non-degradable mutant; however, overexpression of ΔNp63α had little effect on the relative size of otic vesicles (Fig. 5a–d and Supplementary Fig. 7e). Concordantly, *atoh1a* mRNA expression in otic vesicles was eliminated upon thalidomide treatment and was almost fully restored by overexpression of zTAp63α, but not by overexpression of zΔNp63α (Fig. 5e). These results suggest that TAp63α is a major CRL4^{CRBN} target involved in thalidomide-induced developmental defects of otic vesicles.

Discussion

This study illustrates that the *TP63* gene products ΔNp63α and TAp63α are thalidomide-dependent neosubstrates of CRL4^{CRBN} mediating thalidomide teratogenicity (Fig. 6). Remarkably, it seems that ΔNp63α and TAp63α play distinct roles in development and are responsible for thalidomide-induced malformations of fins

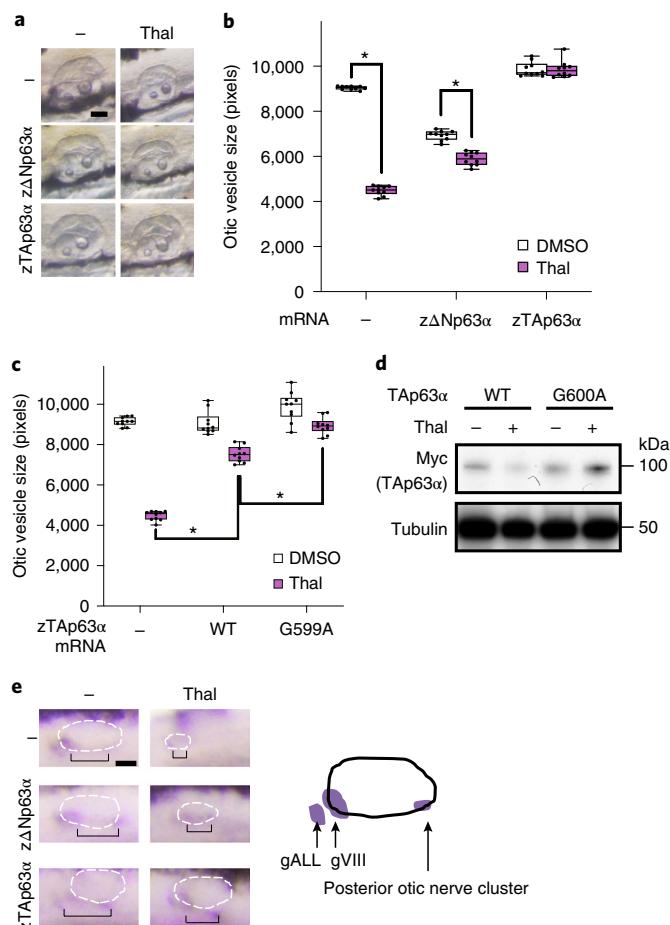


Fig. 5 | Overexpression of zTAp63 reverses thalidomide-induced developmental defects of otic vesicles in zebrafish. a, Close-up views of otic vesicles of 72-hpf embryos uninjected (–) or injected with zΔNp63 or zTAp63 mRNA and developed in the presence or absence of thalidomide. $n = 21$ –34 zebrafish for each group. Scale bar, 50 μm. **b**, Sizes of otic vesicles shown in **a** were measured in pixels and are shown as box-and-whisker plots. Center line, median; box limits, upper and lower quartiles; whiskers, maximum to minimum; dots, individual data points ($n = 10$). Statistical significance was calculated with a two-sided Mann-Whitney U test. * $P < 0.0001$. **c**, Otic vesicle sizes of 72-hpf embryos uninjected (–) or injected with with mRNA encoding wild-type zTAp63 or a G599A variant (the counterpart of hTAp63 G600A) ($n = 10$). Statistical significance was calculated with two-way analysis of variance and Tukey's multiple comparisons test. * $P < 0.0001$. **d**, HEK293T cells overexpressing wild-type TAp63α or a G600A variant were treated with DMSO or thalidomide and harvested for immunoblot analysis ($n = 3$, biological replicates). Full images of blots are shown in Supplementary Fig. 8. **e**, Close-up views of otic vesicles stained with *atoh1a* antisense RNA probe. Zebrafish embryos were treated as in **a** and subjected to in situ hybridization at 48 hpf. The illustration shows cells expressing *atoh1a* in otic vesicles. The white dotted lines indicate otic vesicles. $n = 11$ –23 zebrafish for each group. Scale bar, 50 μm. gALL, anterior lateral line ganglion progenitor; gVIII, statoacoustic ganglion progenitor.

(limbs) and otic vesicles (ears), respectively. Molecular pathways controlling organogenesis and the complex roles of p63 proteins are thought to be well-conserved between humans and zebrafish³³. Consistent with our findings in zebrafish, mutations of *TP63* in humans are associated with congenital limb defects such as ectrodactyly–ectodermal dysplasia cleft lip–palate (EEC) syndrome

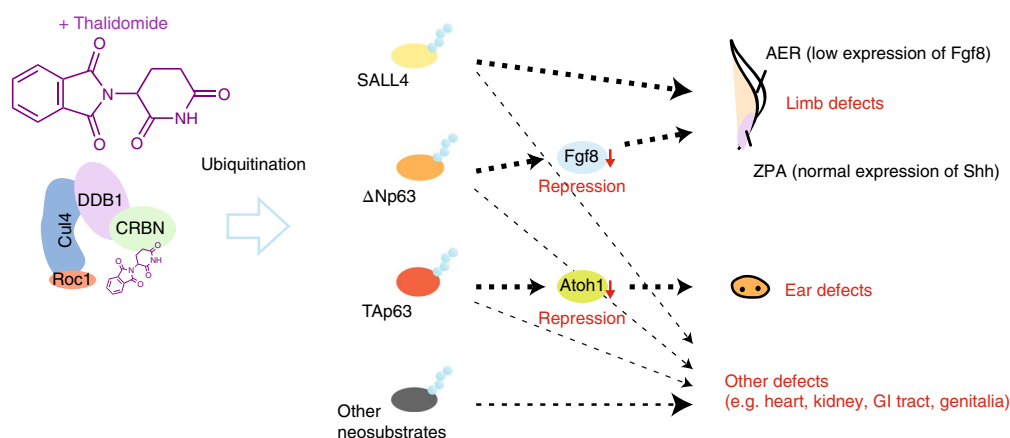


Fig. 6 | Model of the molecular mechanism of thalidomide teratogenicity. When thalidomide binds to CRBN, substrate specificity of CRL4^{CRBN} is altered and CRBN neomorphically binds to ΔNp63, Tap63 and other neosubstrates and ubiquitinates them for proteasomal degradation. The degradation of ΔNp63α causes downregulation of Fgf8a expression in the AER, resulting in developmental defects in fin (limbs), while the degradation of Tap63 causes downregulation of Atoh1 expression, leading to developmental defects in otic vesicles (ears). ZPA, zone of polarizing activity. Shh, Sonic hedgehog.

and acro-dermato-ungual-lacrimal-tooth (ADULT) syndrome. Although TP63-related syndromes and thalidomide embryopathy show a range of clinically overlapping phenotypes, such as limb defects, hearing impairment, dental malformation, kidney hypoplasia and genital malformation, there are some notable differences between these disorders^{15,34}. Whereas mental retardation, autism and ocular anomalies seem to be associated only with thalidomide embryopathy³⁴, common symptoms of TP63-related syndromes such as cleft lip–palate and ectodermal dysplasias are not associated with thalidomide embryopathy. The presence of additional neosubstrates may account for the apparent discrepancy. Recently, SALL4 was identified as a thalidomide-dependent neosubstrate^{13,14}. In humans, SALL4 mutations are associated with Duane radial ray syndrome and Instituto Venezolano de Investigaciones Científicas (IVIC) syndrome, which also show overlapping phenotypes with thalidomide embryopathy and are characterized by limb anomalies and ocular anomalies. It is therefore plausible that SALL4 is also involved in thalidomide-induced limb deformities, adding complexity to its teratogenic effects (Fig. 6). In other words, we assume that p63, SALL4 and perhaps other neosubstrates involved in organogenesis are inhibited by thalidomide to different degrees depending on the timing, dosage and duration of thalidomide exposure, leading to the wide range of limb and other damages seen in thalidomide embryopathy.

Phenotypic differences between TP63-related syndromes and thalidomide embryopathy may be, in part, due to the differences between pharmacological inhibition and genetic mutation. TP63-related syndromes are autosomal dominant disorders. Heterozygous mutation of the TP63 gene would result only in partial inhibition of p63 activity from early embryo to adulthood throughout the body, whereas pharmacological inhibition could result in a more pronounced reduction of p63 activity, but only when the drug is administered and where the drug reaches. Concordant with this assumption, while heterozygous TP63 knockout mice have no obvious abnormalities, homozygous TP63^{-/-} mice show severe ectodermal defects and limb anomalies that are reminiscent of thalidomide embryopathy^{17,35}. Severely truncated forelimbs in TP63^{-/-} mice are quite different from the phenotypes commonly seen in TP63-related syndrome patients such as ectrodactyly or ‘lobster-claw hand’ and syndactyly, suggesting that the level of residual p63 activity affects phenotypic severity of the limbs.

Fgf8 is a critical regulator of limb development whose function is conserved from zebrafish to humans, and accumulating studies have shown that its downregulation leads to the induction of pro-

apoptotic genes and causes cell death in limbs^{6,29}. Here we show evidence suggesting that Fgf8 is a critical downstream effector of the thalidomide–CRL4^{CRBN}–p63 pathway and that thalidomide-induced degradation of ΔNp63α triggers apoptosis through Fgf8 downregulation in the developing limb bud. Alternatively, thalidomide-induced degradation of ΔNp63 may induce apoptosis by enhancing oxidative stress independently of Fgf8. This idea is based on recent papers demonstrating the protective role of ΔNp63α against oxidative-stress-induced cell death^{36,37}. The second model is also consistent with previous studies demonstrating a critical role for oxidative stress in thalidomide action in rabbits^{38,39}. In fact, however, the second model does not conflict with the first model; it is plausible that thalidomide-induced degradation of ΔNp63α increases oxidative stress and that the stress in turn leads to Fgf8 downregulation and induction of proapoptotic genes, triggering apoptosis.

The molecular mechanism by which p63α is recognized by CRBN in a thalidomide-dependent manner is largely unknown. Previous studies have shown that many of the known neosubstrates such as Ikaros, Aiolos, CK1α, GSPT1, GFP91 and SALL4 have a key glycine residue in a β-hairpin in common that is necessary for the recognition by CRBN, although they do not have obvious primary sequence similarity^{8–14}. The critical glycine residue that we identified in p63α is a surface residue of the SAM domain, which is thought to be involved in protein–protein interactions, and is part of a long α-helix in the SAM domain⁴⁰. Therefore, ΔNp63α(G506) and Tap63α(G600) might play a distinct role in CRBN binding from those of the key glycine residues found in other neosubstrates. We showed evidence suggesting that the glycine mutation does not affect the overall structure of p63; however, a complete understanding as to how p63 is recognized by CRBN in a thalidomide-dependent manner and how it is inhibited by the glycine mutation requires elucidation of the CRBN–thalidomide–p63 structure at the atomic resolution.

We and others^{4,24,41–43} have shown that thalidomide treatment and knockdown of CRL4^{CRBN} cause similar pectoral fin defects in zebrafish, leading to the assumption that a thalidomide-sensitive endogenous substrate mediates the teratogenic effect. Here we show, however, that a thalidomide-dependent neosubstrate is responsible for the teratogenic effect. The most likely explanation for the apparent discrepancy is that the phenotypic similarity of thalidomide-treated zebrafish and CRL4^{CRBN}-knockdown zebrafish is coincidental. Unlike in zebrafish, CRBN knockout in mice caused surprisingly weak phenotypes, such as enlarged heart, small liver and decreased vertical activity⁴⁴

(<https://www.mousephenotype.org/data/genes/MGI:1913277>). Thus, developmental roles of CRBN, in the absence of thalidomide, are significantly different between zebrafish and mammals. Then, it follows that thalidomide-induced fin (limb) defects (common to zebrafish and mammals) and CRL4^{CRBN} knockdown-induced fin defects (specific to zebrafish) are similar but distinct, and the presence of a thalidomide-dependent neosubstrate needs to be hypothesized to explain the teratogenic effect. We believe that zebrafish is still a valid model for thalidomide teratogenicity. Despite the difference in CRBN loss-of-function phenotypes between zebrafish and mice, this does not necessarily mean that its gain-of-function phenotypes also vary among species. The use of very high concentrations of thalidomide (100–400 μM) in zebrafish has been criticized by some researchers¹³. Here we showed, however, that direct injection of thalidomide solution into the pectoral fin field of embryos between 24 and 48 hpf results in significant fin defects at 5 μM. Thus, there is no significant difference in effective concentrations between zebrafish and humans.

Recent studies of CRBN have thrown a new light on the development of therapeutic compounds for cancers and inflammatory diseases. In addition to FDA-approved drugs for multiple myeloma such as lenalidomide and pomalidomide, new thalidomide-related compounds targeting CRBN, such as CC-122 (Avadomide) and CC-220 (Iberdomide), have been developed for the treatment of lymphoma and inflammatory diseases^{45,46}. Moreover, synthetic heterobifunctional ligands derived from thalidomide have been successfully used to break down heterologous proteins, such as FKBP12 and BRD4, through CRL4^{CRBN} (refs. 47,48). Considering the growing importance of thalidomide-based drugs targeting CRL4^{CRBN}, it is important to elucidate the molecular mechanism(s) by which some of these compounds exert teratogenic effects. The findings of this study will contribute to the development of new thalidomide-based drugs with reduced or no teratogenic effects.

Online content

Any methods, additional references, Nature Research reporting summaries, source data, statements of code and data availability and associated accession codes are available at <https://doi.org/10.1038/s41589-019-0366-7>.

Received: 8 October 2018; Accepted: 19 August 2019;

Published online: 07 October 2019

References

- Rehman, W., Arfons, L. M. & Lazarus, H. M. The rise, fall and subsequent triumph of thalidomide: lessons learned in drug development. *Ther. Adv. Hematol.* **2**, 291–308 (2011).
- Vargesson, N. Thalidomide-induced teratogenesis: history and mechanisms. *Birth Defects Res. C Embryo Today* **105**, 140–156 (2015).
- Bartlett, J. B., Dredge, K. & Dagleish, A. G. The evolution of thalidomide and its IMiD derivatives as anticancer agents. *Nat. Rev. Cancer* **4**, 314–322 (2004).
- Ito, T. et al. Identification of a primary target of thalidomide teratogenicity. *Science* **327**, 1345–1350 (2010).
- Petroski, M. D. & Deshaies, R. J. Function and regulation of cullin-RING ubiquitin ligases. *Nat. Rev. Mol. Cell Biol.* **6**, 9–20 (2005).
- Moon, A. M. & Capocchi, M. R. Fgf8 is required for outgrowth and patterning of the limbs. *Nat. Genet.* **26**, 455–459 (2000).
- Lewandoski, M., Sun, X. & Martin, G. R. Fgf8 signalling from the AER is essential for normal limb development. *Nat. Genet.* **26**, 460–463 (2000).
- Lu, G. et al. The myeloma drug lenalidomide promotes the cereblon-dependent destruction of Ikaros proteins. *Science* **343**, 305–309 (2014).
- Kronke, J. et al. Lenalidomide causes selective degradation of IKZF1 and IKZF3 in multiple myeloma cells. *Science* **343**, 301–305 (2014).
- Kronke, J. et al. Lenalidomide induces ubiquitination and degradation of CK1α in del(5q) MDS. *Nature* **523**, 183–188 (2015).
- Matyskiela, M. E. et al. A novel cereblon modulator recruits GSPT1 to the CRL4(CRBN) ubiquitin ligase. *Nature* **535**, 252–257 (2016).
- An, J. et al. pSILAC mass spectrometry reveals ZFP91 as IMiD-dependent substrate of the CRL4(CRBN) ubiquitin ligase. *Nat. Commun.* **8**, 15398 (2017).
- Donovan, K. A. et al. Thalidomide promotes degradation of SALL4, a transcription factor implicated in Duane Radial Ray syndrome. *Elife* **7**, e38430 (2018).
- Matyskiela, M. E. et al. SALL4 mediates teratogenicity as a thalidomide-dependent cereblon substrate. *Nat. Chem. Biol.* **14**, 981–987 (2018).
- Rinne, T., Hamel, B., van Bokhoven, H. & Brunner, H. G. Pattern of p63 mutations and their phenotypes—update. *Am. J. Med. Genet. A* **140**, 1396–1406 (2006).
- Restelli, M. et al. DLX5, FGF8 and the Pin1 isomerase control ΔNp63α protein stability during limb development: a regulatory loop at the basis of the SHFM and EEC congenital malformations. *Hum. Mol. Genet.* **23**, 3830–3842 (2014).
- Mills, A. A. et al. p63 is a p53 homologue required for limb and epidermal morphogenesis. *Nature* **398**, 708–713 (1999).
- Boughner, J. C. et al. p63 expression plays a role in developmental rate, embryo size, and local morphogenesis. *Dev. Dyn.* **257**, 779–787 (2018).
- Terrinoni, A. et al. Role of p63 and the Notch pathway in cochlea development and sensorineural deafness. *Proc. Natl Acad. Sci. USA* **110**, 7300–7305 (2013).
- Rouleau, M. et al. TAp63 is important for cardiac differentiation of embryonic stem cells and heart development. *Stem Cells* **29**, 1672–1683 (2011).
- Lapi, E. et al. S100A2 gene is a direct transcriptional target of p53 homologues during keratinocyte differentiation. *Oncogene* **25**, 3628–3637 (2006).
- Ichikawa, T., Suenaga, Y., Koda, T., Ozaki, T. & Nakagawara, A. TAp63-dependent induction of growth differentiation factor 15 (GDF15) plays a critical role in the regulation of keratinocyte differentiation. *Oncogene* **27**, 409–420 (2008).
- Nasevicius, A. & Ekker, S. C. Effective targeted gene 'knockdown' in zebrafish. *Nat. Genet.* **26**, 216–220 (2000).
- Siamwala, J. H. et al. Nitric oxide rescues thalidomide mediated teratogenicity. *Sci. Rep.* **2**, 679 (2012).
- Jiang, L. L. et al. Gambogic acid causes fin developmental defect in zebrafish embryo partially via retinoic acid signaling. *Reprod. Toxicol.* **63**, 161–168 (2016).
- Bakkers, J., Hild, M., Kramer, C., Furutani-Seiki, M. & Hammerschmidt, M. Zebrafish ΔNp63 is a direct target of Bmp signaling and encodes a transcriptional repressor blocking neural specification in the ventral ectoderm. *Dev. Cell* **2**, 617–627 (2002).
- Ando, H. & Okamoto, H. Efficient transfection strategy for the spatiotemporal control of gene expression in zebrafish. *Mar. Biotechnol. (NY)* **8**, 295–303 (2006).
- Chung, F. et al. Thalidomide pharmacokinetics and metabolite formation in mice, rabbits, and multiple myeloma patients. *Clin. Cancer Res.* **10**, 5949–5956 (2004).
- Yu, K. & Ornitz, D. M. FGF signaling regulates mesenchymal differentiation and skeletal patterning along the limb bud proximodistal axis. *Development* **135**, 483–491 (2008).
- Petzold, G., Fischer, E. S. & Thoma, N. H. Structural basis of lenalidomide-induced CK1α degradation by the CRL4(CRBN) ubiquitin ligase. *Nature* **532**, 127–130 (2016).
- Ramsey, M. R., He, L., Forster, N., Ory, B. & Ellisen, L. W. Physical association of HDAC1 and HDAC2 with p63 mediates transcriptional repression and tumor maintenance in squamous cell carcinoma. *Cancer Res.* **71**, 4373–4379 (2011).
- Hans, S., Liu, D. & Westerfield, M. Pax8 and Pax2a function synergistically in otic specification, downstream of the Foxi1 and Dlx3b transcription factors. *Development* **131**, 5091–5102 (2004).
- Saxena, A. & Cooper, K. L. Evolutionary biology: fin to limb within our grasp. *Nature* **537**, 176–177 (2016).
- Miller, M. T. & Stromland, K. Teratogen update: thalidomide: a review, with a focus on ocular findings and new potential uses. *Teratology* **60**, 306–321 (1999).
- Yang, A. et al. p63 is essential for regenerative proliferation in limb, craniofacial and epithelial development. *Nature* **397**, 714–718 (1999).
- Latina, A. et al. ΔNp63 targets cytoglobin to inhibit oxidative stress-induced apoptosis in keratinocytes and lung cancer. *Oncogene* **35**, 1493–1503 (2016).
- Wang, G. X. et al. ΔNp63 inhibits oxidative stress-induced cell death, including ferroptosis, and cooperates with the BCL-2 family to promote clonogenic survival. *Cell Rep.* **21**, 2926–2939 (2017).
- Parman, T., Wiley, M. J. & Wells, P. G. Free radical-mediated oxidative DNA damage in the mechanism of thalidomide teratogenicity. *Nat. Med.* **5**, 582–585 (1999).
- Hansen, J. M., Harris, K. K., Philbert, M. A. & Harris, C. Thalidomide modulates nuclear redox status and preferentially depletes glutathione in rabbit versus rat limb. *J. Pharmacol. Exp. Ther.* **300**, 768–776 (2002).
- Sathyamurphy, A., Freund, S. M., Johnson, C. M., Allen, M. D. & Bycroft, M. Structural basis of p63α SAM domain mutants involved in AEC syndrome. *FEBS J.* **278**, 2680–2688 (2011).
- Zhao, X. et al. Zebrafish cul4a, but not cul4b, modulates cardiac and forelimb development by upregulating tbx5a expression. *Hum. Mol. Genet.* **24**, 853–864 (2015).

42. Beedie, S. L. et al. In vivo screening and discovery of novel candidate thalidomide analogs in the zebrafish embryo and chicken embryo model systems. *Oncotarget* **7**, 33237–33245 (2016).
43. Eichner, R. et al. Immunomodulatory drugs disrupt the cereblon–CD147–MCT1 axis to exert antitumor activity and teratogenicity. *Nat. Med.* **22**, 735–743 (2016).
44. Lee, K. M. et al. Disruption of the cereblon gene enhances hepatic AMPK activity and prevents high-fat diet-induced obesity and insulin resistance in mice. *Diabetes* **62**, 1855–1864 (2013).
45. Hagner, P. R. et al. CC-122, a pleiotropic pathway modifier, mimics an interferon response and has antitumor activity in DLBCL. *Blood* **126**, 779–789 (2015).
46. Matyskiela, M. E. et al. A cereblon modulator (CC-220) with improved degradation of Ikaros and Aiolos. *J. Med. Chem.* **61**, 535–542 (2018).
47. Winter, G. E. et al. Phthalimide conjugation as a strategy for in vivo target protein degradation. *Science* **348**, 1376–1381 (2015).
48. Lai, A. C. & Crews, C. M. Induced protein degradation: an emerging drug discovery paradigm. *Nat. Rev. Drug Discov.* **16**, 101–114 (2017).

Acknowledgements

We thank M. Manabe, M. Akiyama, S. Shoji and K. Taneda for technical assistance. We also thank A. J. Berk for critical comments on this manuscript. This work was supported by MEXT/JSPS KAKENHI grant numbers 17H06112 (to H.H. and Y.Y.), 15H04288 (to H.A.), 17H04213 (to T.I.), 17K14996 (to J.Y.) and 18H05502 (to T.I.). This work was also supported by MEXT-Supported Program for the Strategic Research Foundation at Private Universities S1411011 (to H.H.) and by PRESTO, JST JPMJPR1531 (to T.I.).

Author contributions

T.A.-O. performed most biochemical experiments corresponding to Fig. 1, Fig. 2, Fig. 3e, Fig. 5d, Supplementary Fig. 1, Supplementary Fig. 3 and Supplementary Fig. 6. M.D.S. performed biochemical experiments corresponding to Fig. 1. J.Y. performed biochemical experiments corresponding to Supplementary Fig. 3a. N.S. performed biochemical experiments corresponding to Supplementary Fig. 1g. H.A. and T.S. performed zebrafish experiments corresponding to Fig. 3, Fig. 4, Fig. 5, Supplementary Fig. 4, Supplementary Fig. 5 and Supplementary Fig. 7. T.A.-O., Y.Y., T.I., L.G. and H.H. interpreted all data. H.A. and K.A. interpreted zebrafish data. T.A.-O., T.I., L.G. and H.H. planned this study and wrote the manuscript. L.G. had the initial idea. L.G. and H.H. supervised the project. All authors discussed the results and approved the manuscript.

Competing interests

H.H. has received research support from Celgene Corporation.

Additional information

Supplementary information is available for this paper at <https://doi.org/10.1038/s41589-019-0366-7>.

Correspondence and requests for materials should be addressed to L.G. or H.H.

Reprints and permissions information is available at www.nature.com/reprints.

Publisher's note Springer Nature remains neutral with regard to jurisdictional claims in published maps and institutional affiliations.

© The Author(s), under exclusive licence to Springer Nature America, Inc. 2019

Methods

Cell culture and materials. Human embryonic kidney cell line HEK293T (ATCC) and keratinocyte cell line HaCat (ATCC) were maintained in DMEM (Nacalai Tesque) supplemented with 10% FBS (Biowest) and antibiotic-antimycotic mixed stock solution (Nacalai Tesque). These cell lines were cultured at 37°C with 5% CO₂ and were confirmed to be mycoplasma negative using the MycoAlert Mycoplasma Detection Kit (Lonza).

Plasmids. Plasmids pCMV6-human Δ Np63 α -Myc-FLAG, pCMV6-human Δ Np63 γ -Myc-FLAG and pCMV6-human TAp63 α -Myc-FLAG were purchased from Origene. pcDNA3.1-FLAG-HA-human CRBN was described previously⁴. For FLAG-tagged zCRBN, its cDNA was PCR amplified from zebrafish 24-hpf embryos and cloned into pcDNA3.4 (Thermo Fisher Scientific). Hemagglutinin (HA)-ubiquitin cDNA was cloned into pcDNA3.1. For enhanced GFP (EGFP)-tagged zebrafish (z) Δ Np63 α and (z)TAp63 α , their cDNAs were PCR amplified from 24-hpf embryos and cloned into pCS2 (+) and pcDNA3.4. Point mutations were introduced into the p63 cDNA by overlapping PCR.

Antibodies. Rabbit anti-p63 monoclonal antibody (mAb) (13109, Cell Signaling), rabbit anti-p63 (TA) polyclonal antibody (pAb) (TA327975, ORIGENE), mouse anti-p63 (D-9) mAb (sc-25268, Santa Cruz Biotechnology), rabbit anti-human CRBN65 mAb (Celgene), rabbit anti-ZNF692 pAb (ab204595, Abcam), mouse anti-Myc tag clone 4A6 mAb (05-724, Merck), mouse anti-SALL4 mAb (ab57577, Abcam), anti-HDAC2 [Y461] mAb (ab32117, Abcam), mouse anti- β -actin mAb (ab6276, Abcam) and mouse anti-vinculin mAb (ab18058, Abcam) were used as primary antibodies. Anti-rabbit IgG, HRP-linked Antibody (#7074, Cell Signaling) and anti-mouse IgG, HRP-linked antibody (#7076, Cell Signaling) were used as secondary antibodies. Rabbit anti- α -tubulin pAb-HRP-Direct (PM054-7, MBL), mouse anti-GAPDH-mAb-HRP-Direct (M171-7, MBL), mouse anti-HA-peroxidase mAb (H6533-1VL, Sigma), mouse anti-Myc-tag mAb-HRP-Direct (M192-7, MBL) and mouse anti-DDDDK (FLAG)-tag mAb-HRP-Direct (M185-7, MBL) were also used. Mouse anti-p63 (D-9) mAb (sc-25268, Santa Cruz Biotechnology) and rabbit anti-Myc tag pAb (ab9106, Abcam) were used as primary antibodies, and goat pAb to rabbit IgG Alexa Fluor 488 and to mouse IgG Alexa Fluor 594 (Thermo Fisher Scientific) were used as secondary antibodies for immunocytochemistry.

Co-immunoprecipitation assay. pcDNA3.1-HA-hCRBN and pCMV6- Δ Np63 α -Myc-FLAG were transfected into HEK293T cells using Lipofectamine 2000 (Thermo Fisher Scientific). After 48 h, cells were harvested and lysed with 0.5% NP-40 lysis buffer (50 mM Tris-HCl, 150 mM NaCl and 0.5% NP-40). After centrifugation, cell lysates were incubated with 0.1% DMSO or 100 μ M thalidomide (Tocris Bioscience) for 2 h, followed by 3-h incubation of anti-FLAG M2 agarose beads (A2220, Sigma). The immunoprecipitated complexes were eluted with 3 \times FLAG peptide in lysis buffer and were subjected to immunoblot analysis.

Pull-down assay. Myc-FLAG-tagged Δ Np63 α was transiently transfected into HEK293T cells. The resulting cell lysates were incubated with anti-FLAG M2 magnetic beads (M8823, Sigma) in 0.5% NP-40 lysis buffer and bound Δ Np63 α was eluted with 3 \times FLAG peptide in the same buffer. FLAG-tagged CRBN protein was expressed and purified from Sf9 insect cells as described previously⁴. Δ Np63 α and CRBN proteins (200 ng) were incubated in 0.5% NP-40 lysis buffer containing 0.1 mg ml⁻¹ BSA, together with 0.1% DMSO or 100 μ M thalidomide at 4°C for overnight. After centrifugation, supernatants were incubated with anti-c-Myc magnetic beads (Pierce) for 3 h. Bound proteins were eluted with SDS loading buffer (Nacalai Tesque) and subjected to immunoblot analysis.

Cell-based ubiquitination assay. Wild-type HEK293T or *CRBN*^{-/-} cells were transfected with HA-tagged ubiquitin and Myc-FLAG-tagged Δ Np63 α expression vectors. After 43 h, cells were treated with 0.1% DMSO or 100 μ M thalidomide for 5 h, collected and lysed with RIPA buffer. After centrifugation, cell lysates were incubated with anti-HA magnetic beads (Thermo Fisher Scientific) for 3 h. Bound proteins were eluted by SDS loading buffer and subjected to immunoblot analysis.

Quantitative PCR with reverse transcription. Wild-type HaCat or *CRBN*^{-/-} cells were treated with thalidomide for 24 h. Total RNA was extracted by using RNeasy Plus mini kit (QIAGEN) and reverse transcribed into cDNA using SuperScript IV (Thermo Fisher Scientific). Quantitative PCR was performed in triplicate using the CFX96 Real-Time System (BIO-RAD) and the following primer pairs: β -actin, 5'-GATCGAGAAGGAGATCACTGC-3' and 5'-TACTCTGCTTGCTTGCTGATCCA-3'; and Δ Np63, 5'-AGCCAGAAGAAAGGACAGCA-3' and 5'-TCGTGTACTGTGGCTCACTAA-3'.

Determination of protein half life. HaCat cells were treated with 0.1% DMSO or 100 μ M thalidomide along with 50 ng μ l⁻¹ cycloheximide (Nacalai Tesque) for the indicated time before being collected with RIPA buffer. Cell lysates were subjected to immunoblot analysis.

Immunocytochemistry. HEK293T cells were transfected with wild-type Myc-FLAG-tagged Δ Np63 α or TAp63 α or their nondegrading mutants

and were incubated for 48 h after transfection. The cells were fixed with 4% paraformaldehyde in PBS for 10 min. After blocking for 1 h at room temperature in Bullet Blocking ONE (Nacalai Tesque), the samples were treated with primary antibodies for 16 h at 4°C. The samples were washed and then treated with secondary antibodies for 1 h at room temperature. After washing, the samples were mounted with Vectashield with DAPI and observed with Axio Scope A1 (Zeiss). Fluorescent images were taken by AxioCam ERc 5s (Zeiss).

Breeding of zebrafish embryos. Embryos were collected by natural matings of adult fish that were kept at 28.5°C on a 14 h light–10 h dark cycle. In some cases, embryos were raised in 0.003% phenylthiourea (Sigma) to inhibit pigment formation. The Institutional Animal Care and Use Committee of Tokyo Medical University approved animal use of this study (H290075).

Microinjection into one-cell stage embryos. Capped RNA was dissolved in 0.1% phenol red at 300 ng μ l⁻¹. Antisense morpholino oligonucleotides (MOs) were adjusted to 125–500 μ M. Capped RNA or MOs were loaded into a glass capillary (GD-1, Narishige) and microinjected into the cytoplasm of one-cell stage fertilized embryos at 50 msec release and 30 psi nitrogen gas pressure (IM300, Narishige). MO sequences were as follows: Δ Np63 (for AUG blocking), 5'-TGGTCTCCAGGTACAACATATTGGC-3'; Δ Np63 (for splicing blocking), 5'-ACATTGCTGTATGTCTTACCGTCC-3'; TAp63 (for AUG blocking), 5'-ACTGCTGCATAAGGAGAGGTCATTC-3'; TAp63 (for splicing blocking), 5'-TTTGTAAAGGCACATTACTACTGGT-3'.

In vivo lipofection. In vivo lipofection was performed essentially as described previously²⁷ with some modifications. Four microliters of capped RNA (1,200 ng μ l⁻¹) was mixed with 4 μ l of OPTI-MEM1 (Thermo Fisher Scientific) and 2 μ l of 0.5% phenol red (tube A). In parallel, 3 μ l of Lipofectamine MessengerMAX reagent (Thermo Fisher Scientific) and 7 μ l of OPTI-MEM1 were mixed in a separate tube and placed for 5 min at room temperature (tube B). Solutions A and B were mixed by gentle pipetting and left at room temperature for 20 min. Embryos at 24 hpf were anesthetized and laid on an acrylic plate on its belly, and liposome–RNA complexes were injected to both sides or the left side of the pectoral fin fields. After injection, animals were recovered in E3 medium or fresh breeding water and bred at 28.5°C.

Injection of vivo morpholino. Five microliters of 400 nM VMO (Genes Tools) was mixed with 11 μ l of 0.5% phenol red to adjust the final concentration to 125 nM VMO and injected to both sides or the left side of the pectoral fin fields of 24-hpf embryos. Control VMO, 5'-CCTCTTACTCTCACTTACAATTTATA-3'; Δ Np63 VMO (for AUG blocking), 5'-GTCTCCAGGTACAACATATTGGCGC-3'.

In vivo drug treatment. Thalidomide treatment was performed essentially as described previously⁴ with some modifications. Thalidomide was first added at 6 hpf, and thalidomide solution was replaced every 12 h up to 72 hpf. In some experiments, 280 μ M thalidomide solution containing 0.1% DMSO and 0.1% phenol red was directly injected into the pectoral fin fields at 24 hpf.

Whole-mount in situ hybridization. Whole-mount in situ hybridization was carried out as described previously⁴⁹. The zebrafish *fgf8a* probe was prepared as described previously⁴. The *Atoh1a* probe and *Pax2a* probe used in this study contained the full-length coding sequence of the zebrafish *atoh1a* and *pax2a* gene, respectively.

Alcian blue staining. Extracellular matrices associated with chondrocytes were stained using Alcian blue as described previously⁴. Embryos were fixed in 3.7% neutral buffered formaldehyde at room temperature overnight and then transferred to 0.1% Alcian blue solution in 80% ethanol–20% glacial acetic acid. On the next day, stained embryos were rinsed in absolute ethanol, rehydrated to PBS and cleared with 0.05% trypsin in saturated sodium tetraborate solution for 1–3 h. Pigmentation was removed with 3% hydrogen peroxide–1% potassium hydroxide. Stained embryos were mounted in 70% glycerol–PBS.

Measurement of otic vesicle size. The measurement of otic vesicle size was performed essentially as described previously⁴ with some modifications. First, 24-hpf embryos were anesthetized in 1% methylcellulose containing 0.003% 3-amino benzoic acid ethyl ester (Sigma). The area of otic vesicles was measured using Adobe Photoshop. *P* values were determined using an unpaired *t* test with Welch's correction (GraphPad Prism).

Immunohistochemistry. Embryos were fixed with 4% paraformaldehyde in PBS. After fixation for 90 min at room temperature or overnight at 4°C, embryos were washed with PBS, treated with proteinase K (10 ng μ l⁻¹) in PBS with 0.5% Triton X-100 (PBST) for 15 min at room temperature. Embryos were fixed again to inactivate proteinase K for 15 min at room temperature and blocked with 5% goat serum in PBST for 60 min. Embryos were incubated overnight at 4°C with PBST containing anti-active caspase-3 antibody (#559565, BD Pharmingen; 1:400 dilution) and 5% goat serum and followed by incubation for 4 h at room temperature with PBST containing Alexa Fluor 488 anti-rabbit IgG

antibody (1:2,000 dilution) and 5% goat serum. After washing, embryos were subjected to glycerol immersion (30%, 50% and 75% in PBS). Just before imaging, yolk was removed. Images were taken by using a Lumina Vision OL deconvolution system (Mitani).

Statistical analysis. Each test used for statistical analysis is stated in the figure legends.

Reporting summary. Further information on research design is available in the Nature Research Reporting Summary linked to this article.

Data availability

All data generated or analyzed during this study are included in this published article and its supplementary information or are available from the corresponding author on reasonable request.

References

49. Thisse, C. & Thisse, B. High-resolution in situ hybridization to whole-mount zebrafish embryos. *Nat. Protoc.* **3**, 59–69 (2008).

Reporting Summary

Nature Research wishes to improve the reproducibility of the work that we publish. This form provides structure for consistency and transparency in reporting. For further information on Nature Research policies, see [Authors & Referees](#) and the [Editorial Policy Checklist](#).

Statistics

For all statistical analyses, confirm that the following items are present in the figure legend, table legend, main text, or Methods section.

- | | |
|-------------------------------------|--|
| n/a | Confirmed |
| <input type="checkbox"/> | <input checked="" type="checkbox"/> The exact sample size (n) for each experimental group/condition, given as a discrete number and unit of measurement |
| <input type="checkbox"/> | <input checked="" type="checkbox"/> A statement on whether measurements were taken from distinct samples or whether the same sample was measured repeatedly |
| <input type="checkbox"/> | <input checked="" type="checkbox"/> The statistical test(s) used AND whether they are one- or two-sided
<i>Only common tests should be described solely by name; describe more complex techniques in the Methods section.</i> |
| <input checked="" type="checkbox"/> | <input type="checkbox"/> A description of all covariates tested |
| <input checked="" type="checkbox"/> | <input type="checkbox"/> A description of any assumptions or corrections, such as tests of normality and adjustment for multiple comparisons |
| <input type="checkbox"/> | <input checked="" type="checkbox"/> A full description of the statistical parameters including central tendency (e.g. means) or other basic estimates (e.g. regression coefficient) AND variation (e.g. standard deviation) or associated estimates of uncertainty (e.g. confidence intervals) |
| <input type="checkbox"/> | <input checked="" type="checkbox"/> For null hypothesis testing, the test statistic (e.g. F , t , r) with confidence intervals, effect sizes, degrees of freedom and P value noted
<i>Give P values as exact values whenever suitable.</i> |
| <input checked="" type="checkbox"/> | <input type="checkbox"/> For Bayesian analysis, information on the choice of priors and Markov chain Monte Carlo settings |
| <input checked="" type="checkbox"/> | <input type="checkbox"/> For hierarchical and complex designs, identification of the appropriate level for tests and full reporting of outcomes |
| <input checked="" type="checkbox"/> | <input type="checkbox"/> Estimates of effect sizes (e.g. Cohen's d , Pearson's r), indicating how they were calculated |

Our web collection on [statistics for biologists](#) contains articles on many of the points above.

Software and code

Policy information about [availability of computer code](#)

Data collection

qRT-PCR analysis: CFX96 Real-Time System (Bio-Rad)
Immunocytochemistry: AxioCam ERc 5s (Zeiss)
zebrafish image: BX-51 (Olympus)

Data analysis

Semi-quantitative analysis of WB: ImageJ 1.51s (NIH)
Calculation and statistics: Microsoft Excel for Mac (Microsoft), Prism 8 for mac OS (GraphPad Software)
qRT-PCR analysis: CFX manager (Bio-rad)
Data and images processing: Photoshop CC2019 (Adobe), Illustrator CC2019 (Adobe)

For manuscripts utilizing custom algorithms or software that are central to the research but not yet described in published literature, software must be made available to editors/reviewers. We strongly encourage code deposition in a community repository (e.g. GitHub). See the Nature Research [guidelines for submitting code & software](#) for further information.

Data

Policy information about [availability of data](#)

All manuscripts must include a [data availability statement](#). This statement should provide the following information, where applicable:

- Accession codes, unique identifiers, or web links for publicly available datasets
- A list of figures that have associated raw data
- A description of any restrictions on data availability

The data that support the findings of this study are available from the corresponding author upon reasonable request.

Field-specific reporting

Please select the one below that is the best fit for your research. If you are not sure, read the appropriate sections before making your selection.

- Life sciences Behavioural & social sciences Ecological, evolutionary & environmental sciences

For a reference copy of the document with all sections, see [nature.com/documents/nr-reporting-summary-flat.pdf](https://www.nature.com/documents/nr-reporting-summary-flat.pdf)

Life sciences study design

All studies must disclose on these points even when the disclosure is negative.

Sample size	Group sizes of zebrafish were determined based on the standards in developmental genetic studies using zebrafish.
Data exclusions	No data were excluded.
Replication	Each experiment have been conducted for more than twice in this study and was reproduced.
Randomization	Genetically identical human cultured cells grown under the same conditions were collected, pooled when necessary, and randomly allocated into different experimental groups. Genetically identical zebrafish eggs were collected from the same clutch, pooled when necessary, and randomly allocated into different experimental groups.
Blinding	Blinding was not performed for cell culture experiments. Zebrafish experiments were conducted by two researchers; one performed the experiment, and the other analyzed the data in a blinded fashion.

Reporting for specific materials, systems and methods

We require information from authors about some types of materials, experimental systems and methods used in many studies. Here, indicate whether each material, system or method listed is relevant to your study. If you are not sure if a list item applies to your research, read the appropriate section before selecting a response.

Materials & experimental systems

n/a	Involvement in the study
<input type="checkbox"/>	<input checked="" type="checkbox"/> Antibodies
<input type="checkbox"/>	<input checked="" type="checkbox"/> Eukaryotic cell lines
<input checked="" type="checkbox"/>	<input type="checkbox"/> Palaeontology
<input type="checkbox"/>	<input checked="" type="checkbox"/> Animals and other organisms
<input checked="" type="checkbox"/>	<input type="checkbox"/> Human research participants
<input checked="" type="checkbox"/>	<input type="checkbox"/> Clinical data

Methods

n/a	Involvement in the study
<input checked="" type="checkbox"/>	<input type="checkbox"/> ChIP-seq
<input checked="" type="checkbox"/>	<input type="checkbox"/> Flow cytometry
<input checked="" type="checkbox"/>	<input type="checkbox"/> MRI-based neuroimaging

Antibodies

Antibodies used

For immunoblotting, rabbit anti-p63 monoclonal antibody (mAb) (#13109, Cell Signaling, 1:1000 dilution), rabbit anti-p63 (TA) polyclonal antibody (pAb) (TA327975, ORIGENE, 1:1000 dilution), mouse anti-p63 (D-9) mAb (sc-25268, Santa Cruz Biotechnology, Inc., 1:1000 dilution), rabbit anti-human CRBN65 mAb (Celgene, San Diego, CA, 1:10000 dilution), mouse anti-beta Actin mAb (ab6276, Abcam, 1:2000 dilution), mouse anti-vinculin mAb (ab18058, Abcam, 1:1000 dilution), rabbit anti-ZNF692 pAb (ab204595, Abcam, 1:1000 dilution), mouse anti-Myc tag clone 4A6 mAb (05-724, Merck, 1:1000 dilution), mouse anti-SALL4 mAb (ab57577, abcam, 1:1000 dilution) and anti-HDAC2 [Y461] mAb (ab32117, Abcam, 1:1000 dilution) were used as primary antibodies.

Anti-rabbit IgG, HRP-linked Antibody (#7074, Cell Signaling, 1:10000 dilution) and Anti-mouse IgG, HRP-linked Antibody (7076, Cell Signaling, 1:10000 dilution) were used as secondary antibodies.

Rabbit anti- α -Tubulin polyclonal antibody (pAb)-HRP-Direct (PM054-7, Lot. 006, MBL, 1:5000 dilution), mouse anti-GAPDH-mAb-HRP-Direct (M171-7, Lot. 006, MBL, 1:5000 dilution), rabbit anti-GFP-mpAb-HRP-Direct (598-7, Lot. 005, MBL, 1:1000 dilution), mouse Anti-HA-Peroxidase monoclonal antibody (H6533-1VL, Sigma), mouse anti-Myc-tag mAb-HRP-Direct (M192-7, MBL), and mouse anti-DDDDK (FLAG)-tag mAb-HRP-Direct (M185-7, Lot. 005, MBL, 1:1000 dilution) were also used.

For immunocytochemistry, rabbit anti-Myc tag pAb (ab9106, abcam, 1:200 dilution) and mouse anti-p63 (D-9) mAb (sc-25268, Santa Cruz Biotechnology, Inc., 1:100 dilution) were used as primary antibodies.

Goat pAb to rabbit IgG Alexa Fluor 488 (ab150081, Lot. GR121139-1, abcam, 1:1000 dilution) and to goat pAb to mouse IgG Alexa Fluor 594 (ab150120, Lot. GR177655-1, abcam, 1:1000 dilution) were used as secondary antibodies.

For immunohistochemistry, rabbit anti-active Caspase-3 mAb antibody (#559565, BD Pharmingen, 1:400 dilution) and Alexa Fluor 488 anti-rabbit IgG antibody (1:2000 dilution) were used.

Validation

All the primary antibodies used in the study, except for anti-human CRBN65 mAb, are commercially available. Their reactivity to human antigens and their validity for the applications used are confirmed by the manufacturer. As to anti-

active caspase-3 antibody, its reactivity to zebrafish antigen has been confirmed in several papers (e.g. Ando et al., iScience 2019 doi: 10.1016/j.isci.2019.04.007, and Sato et al. PLoS ONE 2015 doi: 10.1371/journal.pone.0127360). Validity of Anti-human CRBN65 mAb has been confirmed in several reports (e.g. Matyskiela et al., Nature 2016).

Eukaryotic cell lines

Policy information about [cell lines](#)

Cell line source(s)	Parental human embryonic kidney cell line 293T and keratinocyte cell line HaCat were obtained from American Type Culture Collection (ATCC, USA). MM.1S were purchased from ATCC. OPM2 was purchased from JCRB (Japan). RPMI8226, A375-C5, A375-C6 were purchased from ECACC (UK). HCT116 was a gift from Dr. S. Kawai (Toho University). DLD1 was purchased from Horizon Discovery (UK). UM-SCC-14C was purchased from Cell Lines Service(Germany). iPS cells were purchased from Takara-Bio (Japan). HUVEC were purchased from Lonza (Switzerland). Human Cardiac Myocytes were purchased from PromoCell (Germany). The sources of KMS12PE were unknown. Sf9 cells were purchased from Thermo Fisher Scientific (USA).
Authentication	All cell lines used in the experiments were authenticated by PCR analysis.
Mycoplasma contamination	All cell lines were confirmed to be mycoplasma-negative using the MycoAlert Mycoplasma Detection Kit (Lonza).
Commonly misidentified lines (See ICLAC register)	No commonly misidentified cell lines were used.

Animals and other organisms

Policy information about [studies involving animals](#); [ARRIVE guidelines](#) recommended for reporting animal research

Laboratory animals	Commercially available adult zebrafish (<i>Danio rerio</i>) males and females were used for mating. Obtained embryos from 1 hpf to 5 dpf were used for experiments.
Wild animals	No wild animals were involved.
Field-collected samples	No field collected samples were involved.
Ethics oversight	The Institutional Animal Care and Use Committee of Tokyo Medical University approved animal use of this study (H290075).

Note that full information on the approval of the study protocol must also be provided in the manuscript.